Particle induced gamma and X-ray emission spectroscopies of lithium based alloy coatings

Laird, Jamie S.; Hughes, Anthony E.; Ryan, Chris G.; Visser, P.; Terryn, H.; Mol, J. M.C.

DOI
10.1016/j.nimb.2017.03.088

Publication date
2017

Document Version
Accepted author manuscript

Published in
Nuclear Instruments & Methods in Physics Research. Section B: Beam Interactions with Materials and Atoms

Citation (APA)
Laird, J. S., Hughes, A. E., Ryan, C. G., Visser, P., Terryn, H., & Mol, J. M. C. (2017). Particle induced gamma and X-ray emission spectroscopies of lithium based alloy coatings. *Nuclear Instruments & Methods in Physics Research. Section B: Beam Interactions with Materials and Atoms*, *404*, 167-172. https://doi.org/10.1016/j.nimb.2017.03.088

Link to formal publication "Nuclear Instruments and Methods in Physics Research B" (Elsevier):
https://doi.org/10.1016/j.nimb.2017.03.088

NUCLEAR INSTRUMENTS & METHODS IN PHYSICS RESEARCH Section B

Particle Induced Gamma and X-ray Emission Spectroscopies of Lithium Based Alloy Coatings

Jamie S. Laird[*a,b], Anthony E. Hughes [a,c], Chris G. Ryan [a,b], P. Visser [d,e], H. Terryn[d,f] and J. M. C. Mol[d]

[a] *CSIRO, Mineral Resources, Normanby Road, Clayton, Victoria, 3168 Australia*

[b] *School of Physics, University of Melbourne, Parkville, Victoria 3010, Australia*

[c] *Institute of Frontier Materials, Deakin University, Burwood, Victoria 3169 Australia*

[d] *Department of Materials Science and Engineering, Delft University of Technology, Mekelweg 2, 2628 CD Delft, The Netherlands*

[e] *AkzoNobel, Performance Coatings, Rijksstraatweg 31, 2171 AJ Sassenheim, The Netherlands*

[f] *Research Group Electrochemical and Surface Engineering (SURF), Vrije Universiteit Brussel, Pleinlaan 2, 1050 Brussels, Belgium*

Elsevier use only: *Received date here; revised date here; accepted date here*

Abstract: Lithium based inhibitors in aerospace coatings are seen as excellent replacements for their chromium counterparts which are both carcinogenic and heavier. However, Li is generally difficult to detect and following changes in its distribution due to corrosion is impossible with many standard techniques. Combining MeV Particle Induced Gamma Emission and X-ray Emission provides a powerful tool for this research and in this paper we summarise some recent experiments on such coatings using the CSIRO Nuclear Microprobe. PIGE mapping of the $LiCO_3$ particles and their patterning illustrates how the method will be extremely useful in monitoring surface corrosion.

Keywords: m-Particle Induced Gamma-ray Emission (PIGE), Particle Induced X-ray Emission (PIXE), Li coatings, corrosion, Nuclear Microprobe (NMP), corrosion inhibitor, lithium coatings

[*] Corresponding author. e-mail: Jamie.laird@csiro.au.

1. Introduction

The aerospace industry is continually looking to improve performance and reduce CO_2 emissions by making aircraft more fuel efficient. For example, Li is an important alloy component of new generation, high strength-to-weight ratio aluminium alloys which are replacing traditional Al-Cu-Mg alloys. Li replacement of Mg not only makes them lighter but also has improved mechanical properties compared to traditional alloys. However, difficulties in assessing Li distributions with respect to intermetallic inclusions in these alloys remains a technical hurdle. What is not often considered in aircraft design are the longevity and weight of protective coatings such as top paints. Current technology based on hexavalent chromium is carcinogenic and targeted for replacement. Rare earths elements (REE) had been considered as replacements for hexavalent chromium but weight becomes an issue [1]. Recently it has been discovered that Li based corrosion inhibitors are a good alternative [2]. In this paper we summarize 3 MeV m-PIGE and PIXE analysis on Li based coating technology proposed for the protection of aerospace aluminium alloys using the CSIRO Nuclear Microprobe (NMP). Past corrosion studies using PIXE are reported in the literature [3][4].

Unlike REE however, characterizing Li distributions in coatings is problematic for electron beam spectroscopy due to the very low cross-section for *x*-ray production with keV electrons. Auger electrons are the preferred pathway for electronic stopping in this energy regime resulting in overlapped Li and Al peaks. Furthermore, with such a low binding energy any K_α x-rays generated at ~55eV are easily absorbed in the near-surface meaning *any* detected are from the surface and may be dominated by surface sensitive effects *unless* the sample is carefully handled and stored. Transmission Electron Microscopy (TEM) and Electron Energy Loss (EELS) both detect Li but difficult sample preparation and poor detection limits hinder their use. Time of Flight (TOF) SIMS does however provide excellent spatial resolution and sensitivity for Li but scan sizes may be limited.

PIGE on the other hand relies on the detection of prompt gamma rays following nuclear excitation from MeV protons. These gamma rays are primarily from the bulk of the material and surface issues are irrelevant. PIGE is less complicated, more reliable and has excellent detection limits. For these reasons PIGE has found itself indispensable in a range of materials most notably those to do with Li batteries [5]-[7][8], gels[9][10] and thin film technologies [10]-[12][13].

Another key advantage of protons is their long range allowing the primer coating below the topcoat to be probed in plan-view. PIGE is therefore able to measure the spatial distribution of Li and PIXE is able to correlate its relationship with heavier elements in the coating. Not reported here is a more detailed study examining the depletion of Li after exposure to Neutral Salt Spay (NSS), a common corrosion test in the materials industry [14].

2. PIGE and PIXE Methodology

Focused proton beams in the MeV range offer several distinct channels for measuring ^{7}Li in materials. A measurement of alpha particles due to a ^{7}Li (p,α) nuclear reaction or via prompt gamma ray emission from inelastic ^{7}Li(p,$p'\gamma$)^{7}Li pathways [15]. On the CSIRO NMP, the p,$p'\gamma$ pathway with a γ-ray energy of 478 keV is best suited to non-resonant PIGE analysis of geological samples and a large area HPGe gamma detector can be mounted behind the sample [16]. The excitation function for a second γ-ray line at 429keV has a much steeper drop with proton energy below 3 MeV resulting in more surface sensitivity especially in the presence of the heavy metal particles also present in these coating. Overlapping influences from neighbouring γ lines are also minimal for this reaction assuming the Compton background from higher energy γ-rays is removed and there is negligible ^{10}B. Analysis and interpretation of maps is therefore relatively simple. If one irradiates a sample of similar composition, for example LiF, under the same conditions then the ratio of the mass fractions f_m in the unknown i and standard is simply:

$$\frac{f_m^i}{f_m^{st}} = \frac{S^i}{S^{st}} \cdot \frac{Y^i}{Y^{st}} \qquad (1)$$

where *S* and *Y* are the stopping powers and measured yields for the same detector geometry, in the respective sample [17]. For the paint coating cross-sectional analysis, the region to be probed is thicker than the beam range allowing equation (1) to be used. However, proton stopping in the paint is complex due to the nature of the heterogeneous distribution of inclusions containing weight % levels of Ba and Sr. Absolute quantification of the Li levels is not possible as the PIGE excitation function in the standard and paint are dissimilar due to the random granularity of the coatings ($LiCO_3$ and $BaSO_4$). However, the excitation functions and *x*-ray yield distributions both decrease with depth in a similar manner meaning both techniques sample a similar volume of material.

3. Experimental

3.1 Sample Preparation

The AA2024-T3 Al-alloy was used as a substrate for coating. The primer material was a high solids formulation (30 wt%) based on polyurethane with polyisocynate crosslinker [2]. The inorganics included Li_2CO_3 inhibitor, MgO, $BaSO_4$ fillers and TiO_2. The topcoat was polyurethane with binders. The AA2024-T3 was prepared by standard processes used by the aerospace industry beginning with an up to 2 μm thick anodised coating over its surface. After a 24 hr drying period the primer itself was applied by multiple pass spraying to a thickness of 30 μm. The primer was cured at 80 °C for 16 hours. These are then scribed into cross-sectional samples and mounted into conductive Bakelite with the beam to be scanned across the interface between the Al-anodized layer-coating. An SEM Backscattered Electron image of the area under study is shown in Figure 1.

3.2 Ion Beam Analysis

The gamma detector mounted downstream of the sample plane projects into the target chamber to within 5 mm of the sample rear using a re-entrant port. Calibration of the gamma detector uses both a LiF crystal and pure Al. The 100 mm^2 Ge PIXE detector is mounted at 135° and is in close proximity to the sample (~5 mm distance). A 100 μm thick Al filter provided throttling of Al *x*-rays to accentuate heavier element detection limits; Al is picked up in PIGE anyway. A photograph of the system is shown in Figure 2. For the data presented here the *m*DAQ system was used with two channels (PIXE/PIGE) enabled [18]. Scanning areas of approximately 250 μm × 75 μm over the paint cross-section were made. Beam currents of 3 MeV protons were typically in the 0.5-1.0 nA range. Experiments were performed remotely due to the ^7Li (*p*, *n*g) reaction causing a low neutron flux. Post-data collection analysis is performed using GeoPIXE with integrated areas within spectral ROI or "cuts" in the gamma spectrum shown in Figure 3 minus background used to assign pixel values. Shown in the bottom of the same figure is the overall PIXE spectrum and its main fitted contributions.

4. Results

The combined PIXE and PIGE maps for a region of a sample prior to leaching is shown in **Error! Reference source not found.**4. Li, Al, Ag, Ba, Sr, Ti, V and Zr were all detected in the Li-inhibited primer. Li, Ba, Sr and Ti are expected since the primer contains the chemicals Li_2CO_3, $BaSO_4$, $SrSO_4$ and TiO_2. Zr might arise from milling balls (ZrO_2) used to mill the inorganic additives. Al may arise from decoration of voids in the sample during polishing as observed previously using Electron Dispersive Spectroscopy (EDS) on cracks in $SrCrO_4$ particles. Indeed, the distribution of Al within the primer reflects the Ba and Sr maps suggesting these particles may have fractures that capture polishing debris. It should be pointed out that these elements are present in very low levels and it is only through the sensitivity of PIXE that they are detected at all.

With respect to AA2024-T3, typical elements such as Al (PIGE), Cu, Mn and Fe were observed in the matrix and constituent intermetallic particles [19]. Fe was observed only in the constituent particles. The presence of Cu and Mn in the matrix can be explained by a small but significant solubility Cu in Al as well as Cu and Mn being present in a number of intermetallic particles (hardening precipitates and dispersoids) much smaller than the 2 μm beam spot.

Elements such as Ag, Nb, Zr and Zn while not expected may well be low-level alloying additions. Ag is added to facilitate the formation of hardening precipitates which enhances creep resistance, Nb and Zr may form aluminides that act as grain pinners whilst Zn is used for precipitate hardening using the η-phase (Zn_2Mg) in 7xxx series alloys. In this study it is associated with Cu-containing constituent particles and may be present as an impurity from a mixed stock starting material.

5. Discussion

Figure 5 shows three colour maps of the primer region where Li is in red and Ba in blue for all maps and green reflects a changing element. The Li-Cu-Ba map indicates the distribution of the Li- and Ba-containing particles within the primer and the Cu (green) reveals a relationship between the primer and AA2024-T3 substrate. There is a dark band separating the AA2024-T3 from the primer in the Cu map. This same region in the Al map (middle) suggests the strip between the alloy and primer is an anodised layer. The Li-Sr-Ba map shows the red Li-containing particles and the now light blue Ba-containing particles indicating that there is a mixing of the colours associated with the Sr (green) with the Ba (blue) producing the light blue colour.

These maps show that Li is locally concentrated into small regions typically around 7 μm in size, probably reflecting the presence of particles. It is also possible that these particles are further interconnected suggesting clusters of Li_2CO_3. PIXE combined with PIGE conclusively illustrates the complex relationship between intermetallic particles and the Li distribution and appears well capable of measuring spatial changes in these distributions as a function of corrosion.

References

[1] A. E. Hughes and R. J. Taylor, “Chromate conversion coatings on 2024 Al alloy,” *Surface and interface …*, 1997.

[2] P. Visser, Y. Liu, X. Zhou, and T. Hashimoto, “The corrosion protection of AA2024-T3 aluminium alloy by leaching of lithium-containing salts from organic coatings,” *Faraday …*, vol. 180, p. 511, 2015.

[3] A. Boag, R. J. Taylor, T. H. Muster, N. Goodman, D. McCulloch, C. Ryan, B. Rout, D. Jamieson, and A. E. Hughes, “Stable pit formation on AA2024-T3 in a NaCl environment,” *Corrosion Science*, vol. 52, no. 1, pp. 90–103, Jan. 2010.

[4] D. N. Jamieson, S. M. Hearne, and A. E. Hughes, “Combined nuclear microprobe and TEM study of corrosion pit nucleation by intermetallics in aerospace aluminium alloys,” *Nuclear Instruments and …*, 2005.

[5] P. Corvisiero, “PIGE: A Useful Technique for the Study of Innovative Energy Related Materials. Technical Note on the Measurement of Gamma-ray Production Cross Sections,” *Energy Procedia*, vol. 41, pp. 110–118, 2013.

[6] A. Yamazaki, Y. Orikasa, K. Chen, Y. Uchimoto, T. Kamiya, M. Koka, T. Satoh, K. Mima, Y. Kato, and K. Fujita, “In-situ measurement of the lithium distribution in Li-ion batteries using micro-IBA techniques,” *Nuclear Instruments and Methods in Physics Research Section B: Beam Interactions with Materials and Atoms*, vol. 371, pp. 298–302, Mar. 2016.

[7] T. Tadić, M. Jaksic, C. Capiglia, Y. Saito, and P. Mustarelli, “External microbeam PIGE study of Li and F distribution in PVdF/HFP electrolyte gel polymer for lithium battery application,” *Nuclear Instruments and Methods in Physics Research Section B: Beam Interactions with Materials and Atoms*, vol. 161, pp. 614–618, Mar. 2000.

[8] A. Habrioux, S. Surblé, P. Berger, H. Khodja, A. D'Affroux, S. Mailley, T. Gutel, and S. Patoux, “Nuclear microanalysis of lithium dispersion in $LiFePO_4$ based cathode materials for Li-ion batteries,” *Nuclear Instruments and Methods in Physics Research Section B: Beam Interactions with Materials and Atoms*, vol. 290, pp. 13–18, Nov. 2012.

[9] S. Chhillar, R. Acharya, K. B. Dasari, and R. Tripathi, “Proton Induced Gamma-ray Emission Reaction for Quantification of Lithium in Lithium Titanate Samples,” *Proceedings of the DAE …*, 2011.

[10]F. Roux, G. Baud, G. Blondiaux, J. P. Besse, and E. Caudron, “Contribution of nuclear analytical techniques in optimization of Li–Ge–O thin films,” *Solid State Ionics*, 1997.

[11] M. M. Rao, M. Jayalakshmi, O. Schäf, and H. Wulff, “Electrochemical behaviour of solid lithium cobaltate (LiCoO 2) and lithium manganate (LiMn 2 O 4) in an aqueous electrolyte system,” *Journal of Solid State …*, vol. 5, no. 1, p. 50, 2001.

[12] B. Wang, J. B. Bates, F. X. Hart, and B. C. Sales, “Characterization of Thin□Film Rechargeable Lithium Batteries with Lithium Cobalt Oxide Cathodes,” *Journal of The …*, 1996.

[13] H. Benqlilou, “Amorphous lithium cobalt and nickel oxides thin films: preparation and characterization by RBS and PIGE,” *Thin Solid Films*, 1998.

[14] P. Visser , H.A. Terryn, J.M. Mol, Aerospace Coatings, in: A.E. Hughes, J.M. Mol, M.L. Zheludkevich, R.G. Buchheit (Eds.) Active Protective Coatings, New-Generation Coatings for Metals, Springer, Netherlands, 2016, pp. 315-372.

[15] "Analysis of lithium using external proton beams," *Nuclear Instruments and Methods in Physics Research Section B: Beam Interactions with Materials and Atoms*, vol. 15, no. 1, p. 546, Apr. 1986.

[16] C. G. Ryan, D. N. Jamieson, W. L. Griffin, and G. Cripps, "The new CSIRO–GEMOC nuclear microprobe: First results, performance and recent applications," *Nuclear Instruments and …*, 2001.

[17] R. Mateus, A. P. Jesus, and J. P. Ribeiro, "A code for quantitative analysis of light elements in thick samples by PIGE," *Nuclear Instruments and Methods in Physics Research Section B: Beam Interactions with Materials and Atoms*, vol. 229, no. 2, pp. 302–308, Mar. 2005.

[18] J. S. Laird, R. Szymanski, and C. G. Ryan, "A Labview based FPGA data acquisition with integrated stage and beam transport control," *Nuclear Instruments and …*, 2013.

[19] A. E. Hughes, R. Parvizi, and M. Forsyth, "Microstructure and corrosion of AA2024," *Corrosion Reviews*, 2015.

Figures

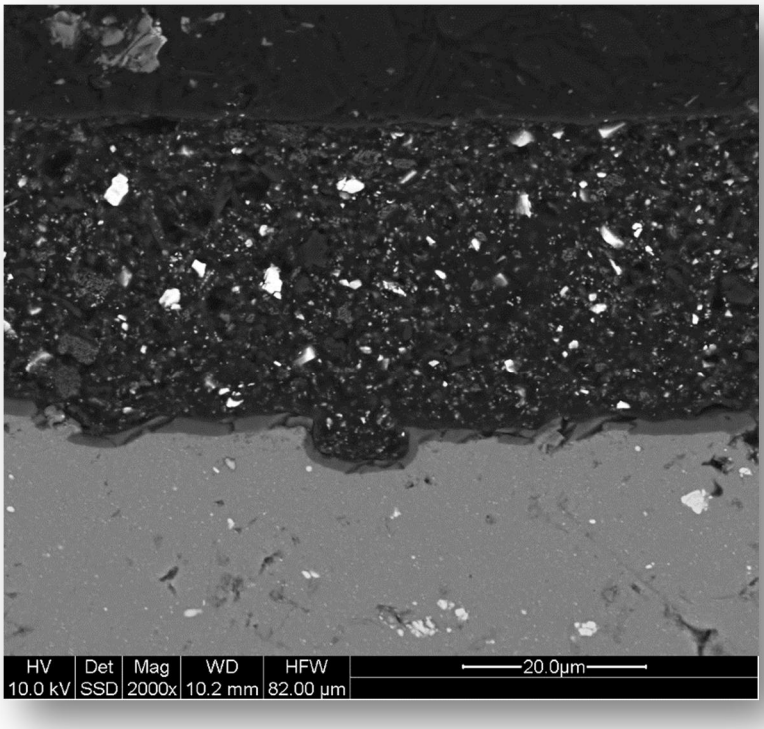

Figure 1: A Backscattered Electron (BSE) image of the interfacial area under study taken on an SEM with conditions stated in the figure. The bottom layer is the Al alloy followed by the 2μm anodized interface. The paint coating can be seen to contain assorted particles and is ~30μm thick. The bright regions are probably intermetallic particles with low average Z.

Figure 2: Photograph of the PIGE/PIXE setup on the CSIRO NMP chamber used for these measurements.

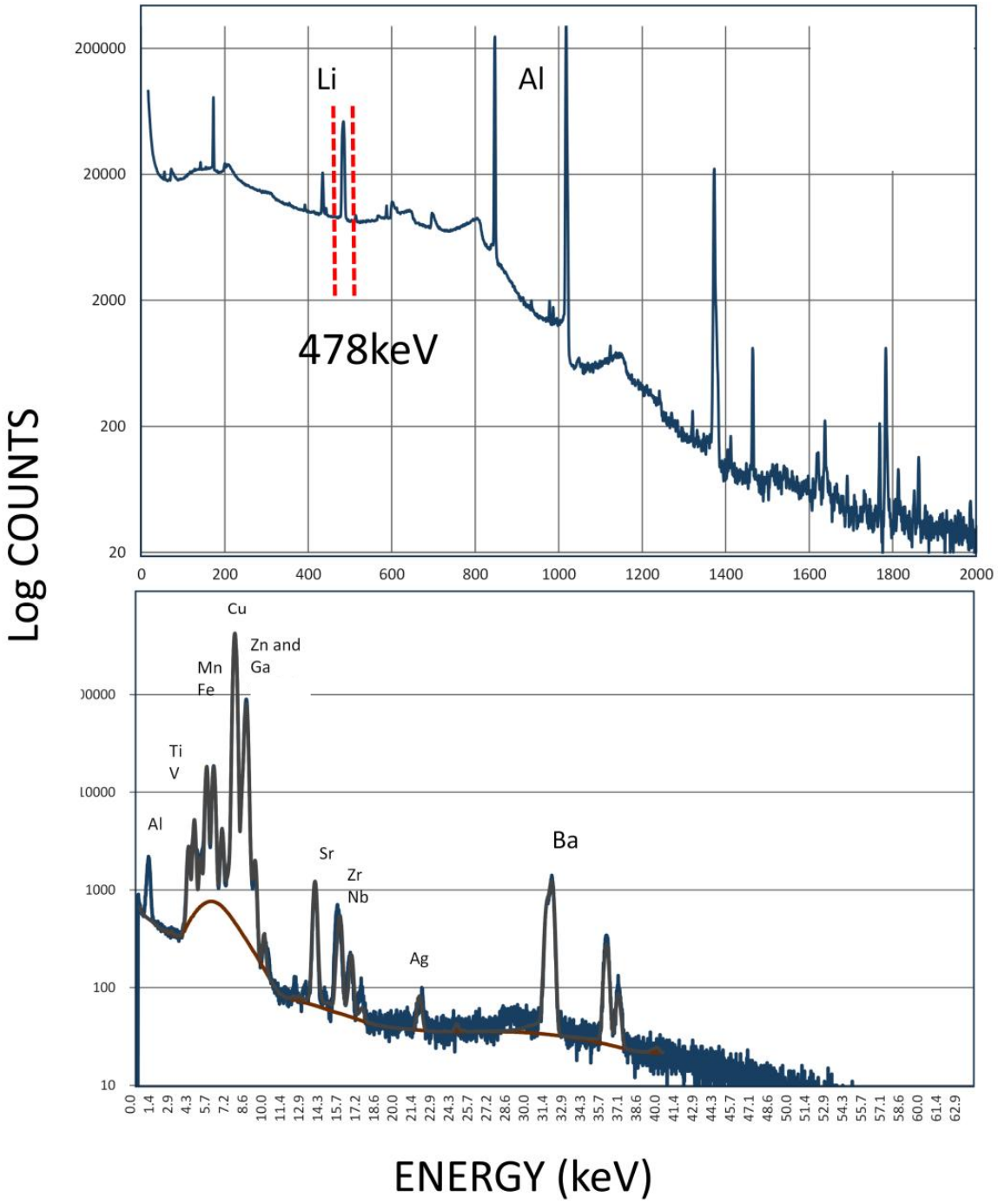

Figure 3: (Top) Typical PIGE spectrum from the alloy coating illustrating the 478 keV Li line used for mapping. The background assumed linear between the two markers is removed for all extracted pixel values (Bottom) The equivalent PIXE spectrum in the same coating region showing the ensemble of elements associated with the Li and Ba particles as well as inter-metallics.

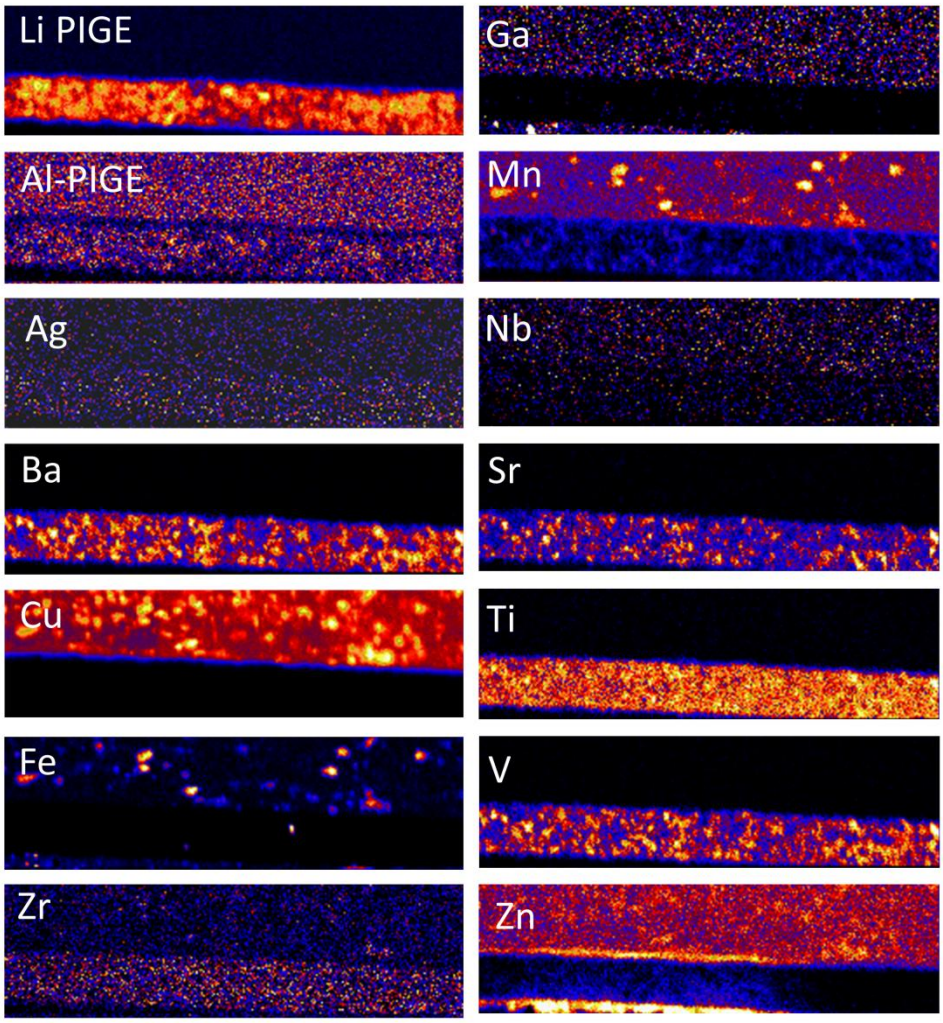

Figure 4: Combined 250 mm x 75 mm PIXE and PIGE maps for an unexposed sample. The PIGE maps (Li and Al) are labelled as such and the rest of the maps are PIXE maps.

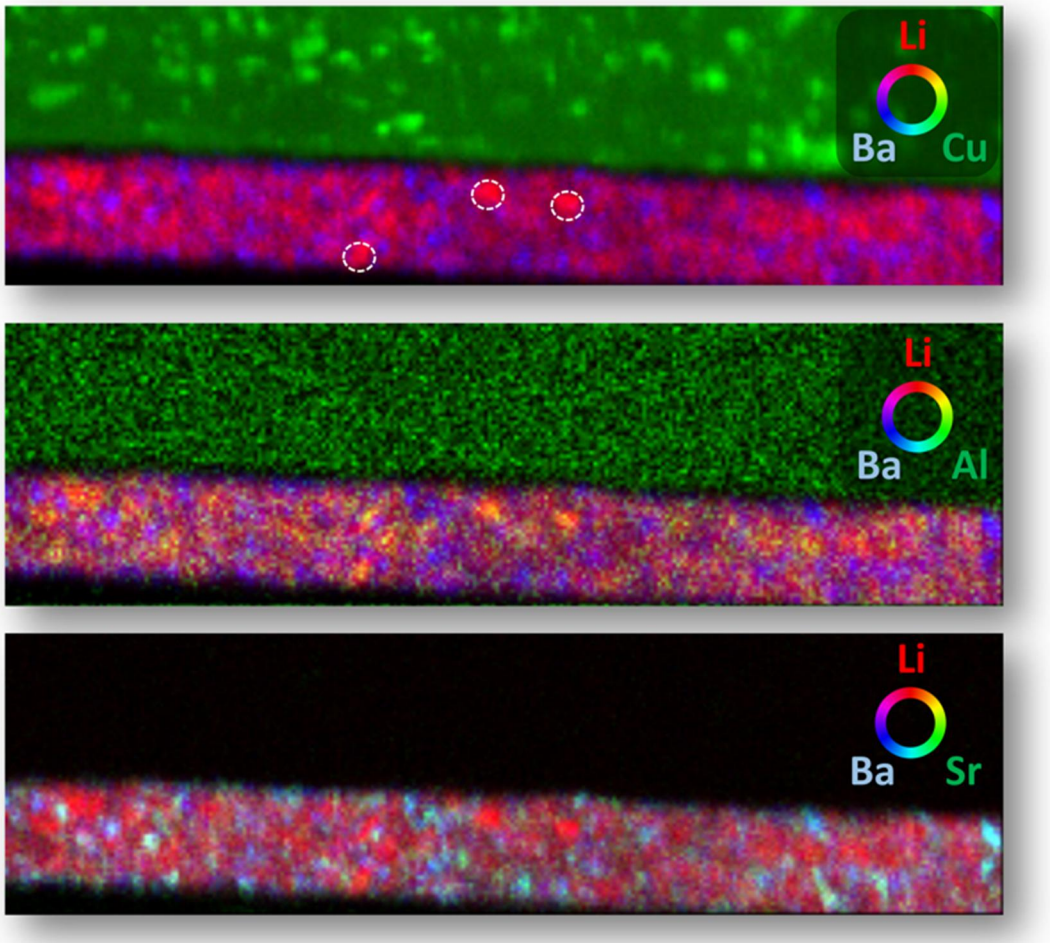

Figure 5: Three colour maps. (Top) Li-Cu-Ba, (middle) Li-Al-Ba and (bottom) Li-Sr-Ba. The red particles in the top plot are Li_2CO_3 particles, typically 7 µm in size.